

# Rotational spectroscopy of S<sub>2</sub>O: vibrational satellites, <sup>33</sup>S isotopomers, and the submillimeter-wave spectrum <sup>★</sup>

S. Thorwirth<sup>a,b,1</sup>, P. Theulé<sup>a,b,2</sup>, C. A. Gottlieb<sup>a,b</sup>,  
H. S. P. Müller<sup>c</sup>, M. C. McCarthy<sup>a,b</sup>, P. Thaddeus<sup>a,b</sup>

<sup>a</sup>*Division of Engineering and Applied Sciences, Harvard University, Cambridge,  
MA 02138, U.S.A.*

<sup>b</sup>*Harvard-Smithsonian Center for Astrophysics, Cambridge, MA 02138, U.S.A.*

<sup>c</sup>*I. Physikalisches Institut, Universität zu Köln, Zùlpicher Str. 77, 50937 Köln,  
Germany*

---

## Abstract

The rotational spectra of disulfur monoxide, S<sub>2</sub>O, and several of its rare isotopic species have been studied in a supersonic molecular beam by Fourier transform microwave spectroscopy. The strongest lines of S<sub>2</sub>O were observed by mixing molecular oxygen with sulfur vapor from a heated reservoir at 190°C, and were so intense that both <sup>33</sup>SSO and S<sup>33</sup>SO were detected in natural abundance, as well as new rotational transitions of <sup>34</sup>SSO and S<sup>34</sup>SO. Vibrationally excited states ( $v_1, v_2, v_3$ ) up to (0, 8, 0), combination states (0,  $v_2, 1$ ) up to (0, 4, 1), and the (1, 0, 0) and (0, 0, 1) states were also observed in a discharge of SO<sub>2</sub> in neon. In addition, the submillimeter-wave spectrum of <sup>32</sup>S<sub>2</sub>O has been studied up to 470 GHz in a free space absorption cell through a discharge of sulfur vapor and SO<sub>2</sub>. An extensive set of molecular parameters for the main isotopic species has been obtained by analyzing all of the presently available rotational and rotation-vibration data.

Detection of several new transitions of the SO dimer S<sub>2</sub>O<sub>2</sub> at centimeter wavelengths has yielded an improved set of molecular parameters for its ground vibrational state.

*Key words:* sulfur oxides, disulfur monoxide, S<sub>2</sub>O, S<sub>2</sub>O<sub>2</sub>, rotational spectroscopy, hyperfine structure, vibrational satellites

*PACS:*

## 1 Introduction

Disulfur monoxide, S<sub>2</sub>O, was first studied spectroscopically in 1959 by Meschi and Myers in the microwave band [1] in a discharge through sulfur vapor and SO<sub>2</sub>. Rotational transitions were detected not only in the ground vibrational state but also in  $v_2 = 1$ . Since then, additional investigations have been carried out at higher frequencies [2,3] and the <sup>34</sup>S isotopomers have been detected [3]. A microwave study of S<sub>2</sub><sup>18</sup>O  $v_2 = 0, 1$  has also been reported [4] as well as diode laser investigations of the  $\nu_1$  (S–O stretching) and  $\nu_3$  (S–S stretching) vibrational bands of S<sub>2</sub><sup>18</sup>O and the main isotopic species, yielding a purely experimental equilibrium structure [5,6]. Highly vibrationally excited S<sub>2</sub>O has been seen in laser-induced fluorescence and cavity ring-down experiments (see e.g. Ref [7]). A summary of the spectroscopic investigations of S<sub>2</sub>O is given by Steudel [8].

In recent radio studies of S<sub>3</sub> and S<sub>4</sub> in this laboratory [9–11], fairly strong lines of S<sub>2</sub>O were observed as an impurity, prompting us to undertake a new study of this molecule, deliberately adding molecular oxygen or sulfur dioxide to the source to produce even stronger lines. This new study, which greatly extends the previous work, includes: (i) a Fourier transform microwave (FTM) investigation of rotational transitions of S<sub>2</sub>O in the ground vibrational state as well as vibrational satellites from  $(v_1, v_2, v_3) = (1, 0, 0)$ ,  $(0, 0, 1)$ ,  $(0, v_2, 0)$  up to  $v_2 = 8$ , and the combination modes  $(0, v_2, 1)$  up to  $v_2 = 4$ ; (ii) an FTM investigation of the mono <sup>34</sup>S and <sup>33</sup>S isotopic species; and (iii) a millimeter and submillimeter wave investigation of S<sub>2</sub>O in the ground vibrational state to frequencies as high as 470 GHz.

## 2 Experimental

The FTM spectrometer used in the present investigation, described in detail elsewhere [12,13], operates between 5 and 42 GHz. Transient molecules are produced in the throat of a pulsed nozzle through a stream of appropriate precursor gases heavily diluted in a buffer gas (typically Ne or Ar). Free expansion from the nozzle into the large vacuum chamber of the spectrometer

---

\* This work is dedicated to Prof. Dr. Gisbert Winnewisser on the occasion of his 70<sup>th</sup> birthday, in recognition of his many contributions to laboratory astrophysics and radio astronomy.

<sup>1</sup> Present address: Max-Planck-Institut für Radioastronomie, Auf dem Hügel 69, 53121 Bonn, Germany.

<sup>2</sup> Present address: Physique des interactions ioniques et moléculaires, Université de Provence, Centre de Saint Jérôme, 13397 Marseille Cedex 20, France.

forms a supersonic beam moving at about twice the speed of sound. As the molecules approach the center of the Fabry-Perot cavity, rotational transitions are excited by a short pulse of resonant microwave radiation. Transient line emission from the coherently rotating molecules is then detected by a sensitive microwave receiver, and the Fourier transform of this decaying signal then yields the desired power spectrum. In the present experimental configuration with the molecular beam oriented along the axis of the Fabry-Perot cavity, each line is split into two well-resolved Doppler components corresponding to the two traveling waves which compose the standing wave of the Fabry-Perot mode.

With a discharge, fairly strong lines of S<sub>2</sub>O are produced from SO<sub>2</sub> (0.2% in neon), but even stronger ones are obtained without a discharge by simply mixing molecular oxygen (0.2% in neon) with sulfur vapor at a temperature of about 190°C (using the same heated nozzle as in our recent study of S<sub>3</sub> and S<sub>4</sub>). This technique was used to study the ground state rotational spectra of S<sub>2</sub>O and its mono-<sup>34</sup>S and <sup>33</sup>S isotopic species (the latter for the first time). The real purpose of a discharge in the present work is to vibrationally excite S<sub>2</sub>O, and to allow us to measure vibrational satellites in the rotational spectrum (see e.g. Ref. [14]). Using this method, vibrational satellites of S<sub>2</sub>O from a total of fourteen vibrational states were observed. Source conditions were a stagnation pressure behind the pulsed valve of 3.5 atm and a discharge potential of 1.0 – 1.3 kV.

The millimeter-wave study of S<sub>2</sub>O was done with the free-space absorption spectrometer in this laboratory [15]. In this instrument, millimeter-wave radiation is generated by a solid-state Gunn oscillator, and then multiplied in frequency to yield useful carrier signals to 500 GHz and beyond. In the present work, experimental parameters were very similar to those adopted for our recent investigation of S<sub>3</sub> and S<sub>4</sub> [11], except that a dilute mixture of SO<sub>2</sub> in argon was used instead of pure argon to increase the amount of oxygen.

The rare isotopic species of S<sub>2</sub>O were studied in natural abundance, nearly all only with the FTM spectrometer because of its superior sensitivity.

### 3 Analysis

Like isovalent SO<sub>2</sub> and S<sub>3</sub>, S<sub>2</sub>O is bent, with the structural equilibrium parameters  $d_{SS} = 188.4$  pm,  $d_{SO} = 145.6$  pm and  $\alpha_{SSO} = 117.88^\circ$  [6]. Owing to the lower symmetry ( $C_S$  instead of  $C_{2v}$ ) S<sub>2</sub>O exhibits both *a*- and *b*-type transitions. The two dipole moment components  $\mu_a = 0.875(10)$  D and  $\mu_b = 1.18(2)$  D [1] are comparably strong, leading to a fairly dense rotational spectrum dominated by strong *b*-type *Q*-branch and *a*- and *b*-type *R*-branch

progressions.

In the least-squares analyses, Pickett's program SPFIT [16] with Watson's Hamiltonian in the  $A$ -reduction was used throughout. In all tables,  $1\sigma$  uncertainties (in parentheses) are given in units of the last significant digits.

### 3.1 The main species, $^{32}\text{S}_2\text{O}$

Very strong lines of  $\text{S}_2\text{O}$  in the ground and  $(0, 1, 0)$  bending vibrational state were observed with the FTM spectrometer in a discharge through  $\text{SO}_2$  in neon. A survey scan around the fundamental  $a$ -type transition  $1_{0,1} - 0_{0,0}$  at 9566 MHz revealed more than 10 satellites from vibrational states whose pure rotational spectra had not previously been observed (Figure 1). Rotational transitions from the first excited stretching modes  $(1, 0, 0)$  and  $(0, 0, 1)$  were readily identified on the basis of frequencies calculated with constants determined from a fit to the rotation-vibration data in Lindenmayer et al. [5,6]. In all, 46 lines for the ground and first excited vibrational states (Table 1), and 61 lines from overtones of  $\nu_2$  with  $2 \leq v_2 \leq 8$  and combinations modes of  $\nu_2$  and  $\nu_3$  with  $v_2 \leq 4$ , were measured in the centimeter-wave band (Table 2).

Following the FTM investigation, a millimeter/submillimeter wave study of the ground vibrational state was undertaken at frequencies as high as 470 GHz. Prior to this work, rotational lines of  $\text{S}_2\text{O}$  had not been measured above 140 GHz [2]. A total of 139 lines were measured (see Table 3; unresolved asymmetry doublets are counted only once). Sample spectra showing  $a$ -type  $R$ -branch transitions that are rather close to oblate pairing are shown in Figure 2.

Two sets of spectroscopic parameters of  $^{32}\text{S}_2\text{O}$  are given in Table 4. In Fit 1, the constants for the ground state were obtained from the pure rotational data of the  $(0, 0, 0)$  state, the rotation-vibration data of the  $(1, 0, 0)$  and  $(0, 0, 1)$  states and the vibrational satellite data of the latter two states. In Fit 2, all pure rotational and rotation-vibration data presently available were analyzed in a global fit in which each rotational and centrifugal distortion constant  $X_v$  in the Hamiltonian has the following general form:

$$X_v = X_e + \sum_{i=1}^3 \alpha_i^X \left( v_i + \frac{1}{2} \right) + \sum_{i,j=1}^3 \beta_{ij}^X \left( v_i + \frac{1}{2} \right) \left( v_j + \frac{1}{2} \right) + \sum_{i,j,k=1}^3 \gamma_{ijk}^X \left( v_i + \frac{1}{2} \right) \left( v_j + \frac{1}{2} \right) \left( v_k + \frac{1}{2} \right) + \dots, \quad (1)$$

where the subscripts  $i$ ,  $j$ , and  $k$  refer to the corresponding vibrational modes.

Equation (1) is an extension of the Dunham expressions for a diatomic molecule (see e.g. Ref [17]). In this case, one also finds the following alternative expressions besides Dunham’s formulation:

$$B_v = B_e - \alpha_e \left( v + \frac{1}{2} \right) + \gamma_e \left( v + \frac{1}{2} \right)^2 + \dots \quad (2)$$

$$D_v = D_e + \beta_e \left( v + \frac{1}{2} \right) + \delta_e \left( v + \frac{1}{2} \right)^2 + \dots \quad (3)$$

These expressions do not accommodate vibrational corrections to sextic or higher-order centrifugal distortion parameters, so for an asymmetric rotor such as S<sub>2</sub>O a more general formulation as given in Eq. (1) is useful. The parameters in Eq. (2) and (3) are related to the ones in Eq. (1); e.g.  $-\alpha_e$  in Eq.(2) corresponds to  $\alpha^B$  in Eq. (1). More specifically, each  $-\alpha_e$  and  $\beta_e$  in Eq. (2) and (3) has a corresponding  $\alpha_i^X$  in Eq. (1) and each  $\gamma_e$  and  $\delta_e$  in Eq. (2) and (3) has a corresponding  $\beta_{ij}^X$  in Eq. (1), and so on.

The new set of spectroscopic constants for <sup>32</sup>S<sub>2</sub>O are given in Table 4. The largest number of vibrational corrections was needed for the  $\nu_2$  mode, because lines were measured in states with up to eight quanta. The terms  $\gamma_{223}^{B,C}$  were necessary in the treatment of the combination modes (0,  $\nu_2$ , 1), but only the  $\alpha_1^X$  terms were required in the analysis of the S–O stretching mode  $\nu_1$  because only the first excited state was observed. In the global analysis (Fit 2), the vibrational dependence is largest for the rotational constants  $A$ ,  $B$ , and  $C$ . Generally, differences for  $\alpha_v^{A,B,C}$  in Table 4 and  $-\alpha_v^{A,B,C}$  in Ref. [6] are quite small ( $< 200$  kHz), except for  $\alpha_2^A$  which differs by about 18 MHz owing to inclusion of  $\beta_{22}^A$  in the present work. For the quartic centrifugal distortion constants three, four, and four rotation-vibration interaction constants  $\alpha_i^X$  could be determined for the  $\nu_1$ ,  $\nu_2$ , and  $\nu_3$  modes, respectively, since the differences between the ground state spectroscopic constants (Fit 1) and the corresponding near-equilibrium constants (Fit 2) are well determined.

In the case of high-order constants virtually no vibrational dependence can be determined from the present data, so  $X_0$  and  $X_e$  are nearly the same.

### 3.2 <sup>34</sup>SSO and S<sup>34</sup>SO

The two singly substituted <sup>34</sup>S isotopic species were readily observed in the FTM spectrometer near frequencies predicted from the data reported by Tie-mann et al. [3]. As summarized in Table 5, 15 lines of <sup>34</sup>SSO and 14 of S<sup>34</sup>SO were measured in the microwave range up to 39 GHz. The most intense lines were recorded in a discharge of SO<sub>2</sub> in neon. Lines which were weak in the dis-

charge source were then measured in the hot sulfur/molecular oxygen source. We did not attempt to detect vibrational satellites of the  $^{34}\text{S}$  isotopomers in our discharge source, but that could almost certainly be done. Transition frequencies for both isotopomers were calculated with the new set of spectroscopic constants, and another 24 lines of  $^{34}\text{SSO}$  and 27 lines of  $\text{S}^{34}\text{SO}$  were measured in the 90 GHz region, most of which are either  $b$ -type  ${}^rQ_1$  or  $a$ -type ( $J = 10 - 9$ )  $R$ -branch transitions (Table 6). A combined fit of the data in Ref. [3] and the new data (Tables 5 and 6), yields an improved sets of spectroscopic constants (Table 7): all five quartic centrifugal distortion constants and one sextic constant ( $\Phi_{KJ}$ ) have now been determined for both isotopomers. Additional sextic and octic centrifugal distortion constants were taken from  $^{32}\text{S}_2\text{O}$  (Table 4, Fit 1) and kept fixed.

### 3.3 $^{33}\text{SSO}$ and $\text{S}^{33}\text{SO}$

The intensity of the  $\text{S}_2\text{O}$  lines in the hot sulfur/oxygen source was sufficiently high to undertake a search for the  $1_{0,1} - 0_{0,0}$  transitions of the two singly substituted  $^{33}\text{S}$  isotopomers in natural abundance (0.75%). Initially, the search was based on scaled rotational constants obtained by comparing the equilibrium and ground state rotational constants of the main isotopic species and multiplying these correction factors with the equilibrium rotational constants of  $^{33}\text{SSO}$  and  $\text{S}^{33}\text{SO}$ . A somewhat more sophisticated estimate can be obtained from rotational parameters evaluated from an  $\text{S}_2\text{O}$   $r_{I,\epsilon}$  structure [18]. Here, it is assumed that vibrational contributions  $\epsilon_i$  to the ground state moments of inertia  $I_{0,i}$  are the same for each isotopic species. The interesting aspect of this structural model is that it predicts ground state rotational constants of new isotopic species rather well because of the explicit determination of  $\epsilon_i$  (for example see Ref. [19]). Employing data for  $^{32}\text{S}_2\text{O}$ ,  $^{34}\text{SSO}$ ,  $\text{S}^{34}\text{SO}$  (this study) and  $\text{S}_2^{18}\text{O}$  [4,6], first estimates of the  $B_i$  were determined for  $^{33}\text{SSO}$  and  $\text{S}^{33}\text{SO}$ . The structural fit had residuals for  $B$  and  $C$  of less than 100 kHz while those of the much larger  $A$  constant were less than 750 kHz. The best estimates of the rotational parameters of the  $^{33}\text{S}$  isotopic species were obtained by correcting the initial estimates on the assumption that the residuals of  $^{33}\text{SSO}$  and  $\text{S}^{33}\text{SO}$  in a structural fit lie between those of  $\text{S}_2\text{O}$  and the corresponding  $^{34}\text{S}$  isotopic species (Table 9). Effects of centrifugal distortion on the low- $J$  transitions are small, nevertheless to further improve our estimates for rotational transitions of the  $^{33}\text{S}$  isotopic species, we assumed that the quartic distortion constants are the mean of the normal and  $^{34}\text{S}$  isotopic species. In addition,  $^{33}\text{S}$  nuclear quadrupole coupling constants were calculated at the B3LYP/cc-pCVTZ level of theory (GAUSSIAN03 [20], Table 9).

Guided by these estimates of the transition frequencies the two sulfur-33 isotopic species were detected in the supersonic beam. The spectra shown in

Figure 3 are aligned on the strong central ( $F = 2.5 - 1.5$ ) hyperfine component to illustrate the differences in the hyperfine structure (hfs) of the two isotopic species. The upper spectrum is the result of about 25 minutes of integration time. In addition to the three hfs components of the  $1_{0,1} - 0_{0,0}$  transition, six hfs components of the  $2_{0,2} - 1_{0,1}$  transition were also measured for both molecules. The experimental transition frequencies are summarized in Table 8, which also gives the transition frequencies of four hfs components of the  $6_{1,6} - 5_{0,5}$   $b$ -type transition of  $^{33}\text{SSO}$  that were observed at 88 GHz and helped to determine its  $A$  rotational constants.

Observation of the  $1_{0,1} - 0_{0,0}$  and  $2_{0,2} - 1_{0,1}$  transitions of the prolate asymmetric rotors  $^{33}\text{SSO}$  and  $\text{S}^{33}\text{SO}$  with almost all of its hfs components yields  $B + C$ ,  $\chi_{aa}$ , and  $C_{bb} + C_{cc}$ . The effects of asymmetry in  $^{33}\text{SSO}$  and  $\text{S}^{33}\text{SO}$  are very small in the  $2_{0,2} - 1_{0,1}$  transition, nevertheless they are large enough to allow the determination of  $\chi_{bb}$  for both isotopic species but the uncertainty in  $\chi_{bb}$  is about two orders of magnitude larger than that of  $\chi_{aa}$ . The effects of centrifugal distortion are small enough and asymmetry are large enough to yield  $B$  and  $C$  separately rather than  $B + C$  and  $\Delta_J$ .

The two sets of rotational parameters of  $^{33}\text{SSO}$  and  $\text{S}^{33}\text{SO}$  are shown in Table 9. As can be seen the rotational constants from the  $r_{I,\epsilon}$  structure show very good agreement with the experimentally determined values. Comparison of the theoretical and measured nuclear quadrupole coupling constants confirms that the B3LYP/cc-pCVTZ calculation provides a reliable estimate that is accurate to within 10%.

### 3.4 $\text{S}_2\text{O}_2$

The rotational spectrum of  $\text{S}_2\text{O}_2$  (connectivity: OSSO) was first observed by Lovas et al. [21] in a discharge of  $\text{SO}_2$ . In analogy to its isovalent pure sulfur analog  $\text{S}_4$ , the molecule has  $C_{2v}$  symmetry with the two SO moieties arranged in a trapezoidal, *cis*-planar configuration. Several transitions of  $\text{S}_2\text{O}_2$  were observed at centimeter wavelengths in the discharge of  $\text{SO}_2$ , including six new transitions and four that were remeasured to much higher accuracy than before (Table 10). The derived spectroscopic constants (Table 11) were obtained in two different fits, one based solely on the data in Ref. [21] and the other from a combined fit of the measurements in Table 10 with those in Ref. [21]. Uncertainties in the rotational constants are an order of magnitude smaller and the centrifugal distortion constants are better determined in the combined fit.

## 4 Discussion

The present study greatly extends the available laboratory rotational data on S<sub>2</sub>O. The detection of vibrational satellites from states as high as  $\approx 3000 \text{ cm}^{-1}$  (4400 K) above ground emphasizes how well a discharge produces vibrationally hot S<sub>2</sub>O, and it is clear that many more vibrational satellites might be detected by the present techniques. Table 12 contains predictions for selected vibrational satellites of S<sub>2</sub>O in twelve states not studied here. Detection of these would significantly improve the rotation-vibration parameters of S<sub>2</sub>O.

The present FTM work also yields new data on the mono-<sup>34</sup>S and -<sup>33</sup>S isotopic species. The nuclear quadrupole coupling constants obtained from quantum chemical calculations at the B3LYP/cc-pCVTZ level of theory are in good agreement with those derived from our measurements. Since the orientation of the electric field gradient principal axes of S<sup>33</sup>SO differs little from that of <sup>33</sup>SO<sub>2</sub>, it is not surprising that the quadrupole constants are also similar, both in sign and magnitude (S<sup>33</sup>SO vs. <sup>33</sup>SO<sub>2</sub>:  $\chi_{aa} = -5.8$  vs  $-1.8$  MHz,  $\chi_{bb} = 22.2$  vs.  $25.7$  MHz,  $\chi_{cc} = -16.4$  vs.  $-23.9$  MHz; <sup>33</sup>SO<sub>2</sub> data taken from Ref. [22])<sup>3</sup>. Differences in the electronic environment of the central sulfur atom are evident however in  $\chi_{cc}$ , since the *c* inertial axes in S<sub>2</sub>O and SO<sub>2</sub> are collinear. Because of the different orientations of the molecules in the *ab* planes, direct comparison of  $\chi_{aa}$  and  $\chi_{bb}$  is of limited value. The off-diagonal coupling constants  $|\chi_{ab}|$  were calculated theoretically to be roughly 11 and 7 MHz for <sup>33</sup>SSO and S<sup>33</sup>SO, respectively, but they could not be determined experimentally. Additional rotational data on the <sup>33</sup>S isotopic species, especially *b*-type transitions and *a*-type transitions with  $K_a > 0$ , would be of help in determining the *A* rotational constant of S<sup>33</sup>SO experimentally.

The two sets of rotational constants of the main isotopic species <sup>32</sup>S<sub>2</sub>O in Table 4 require a brief consideration. For a planar molecule in its equilibrium configuration, the inertial defect  $\Delta_e = I_c^e - I_b^e - I_a^e = 0$ . The ground state moments of inertia usually yield a small positive value  $\Delta_0$ , owing to contributions from (i) zero-point vibration, (ii) centrifugal distortion, and (iii) electron-rotation interaction, i.e.,  $\Delta_0 = \Delta_{vib} + \Delta_{cent} + \Delta_{elec}$  [23]. Lindenmayer et al. [6] derived a value of  $\Delta_e = -0.0075 \text{ amu } \text{Å}^2$  for S<sub>2</sub>O, but their estimate still contains contributions from higher-order rotation-vibration and electron-rotation interactions. In the present investigation, information about higher-order rotation-vibration interaction has been obtained (Table 4, Fit 2). To evaluate the inertial defect, the rotational equilibrium constants have been corrected for small effects of quartic centrifugal distortion as outlined in Ref.

---

<sup>3</sup> It may be noted that a DFT calculation with a smaller basis set (B3LYP/cc-pVTZ) also yields good results: <sup>33</sup>SSO:  $\chi_{aa} = -15.5$  MHz,  $\chi_{bb} = 33.0$  MHz,  $\chi_{cc} = -17.5$  MHz; S<sup>33</sup>SO:  $\chi_{aa} = -5.4$  MHz,  $\chi_{bb} = 22.0$  MHz,  $\chi_{cc} = -16.6$  MHz.



[23].  $\Delta_{cent} = 0.0009 \text{ amu } \text{\AA}^2$  has been derived from the quadratic force field (cf. Ref. [24]). Our estimate of  $\Delta_{elec} = -0.0052 \text{ amu } \text{\AA}^2$  is somewhat larger than  $\Delta_{elec} = -0.0037 \text{ amu } \text{\AA}^2$  determined for  $\text{SO}_2$  [25], but it may still depend on further higher-order vibration-rotation contributions owing to uncertainties in  $\Delta_{vib}$  and  $\Delta_{cent}$ . Further refinement in this estimate would require extending the measurements to energetically higher vibrational states and to higher frequencies.

$\text{S}_2\text{O}$  is a plausible candidate for astronomical detection. Over ten percent of the molecules detected in space so far contain sulfur<sup>4</sup> and the oxides  $\text{SO}$  and  $\text{SO}_2$  are particularly abundant, especially in star-forming regions such as Orion, where line emission from  $\text{SO}_2$  is found to contribute substantially to the cooling of the molecular gas [27].  $\text{S}_2\text{O}$  may also be present in comets, where  $\text{S}$ ,  $\text{S}_2$ ,  $\text{SO}$ , and  $\text{SO}_2$  have already been detected [28]. It is a plausible constituent of planetary atmospheres such as that of Venus [29] or Jupiter’s Galilean moon Io where it is thought to be released into the atmosphere by volcanic eruptions or formed by photochemical reactions [30–32]. The laboratory data on  $\text{S}_2\text{O}$  discussed here should allow very sensitive radio astronomical searches for this molecule, both with large single-dish telescopes and with present interferometers. Frequency predictions as well as the global fit file of  $\text{S}_2\text{O}$  can be found online at the CDMS at <http://www.cdms.de>.

Searches for other exotic sulfur oxides in our molecular beam are worth doing. To date, trisulfur monoxide,  $\text{S}_3\text{O}$ , has only been observed by mass spectrometry [33] which does not yield the molecular structure. Recent *ab initio* calculations indicate that a branched  $C_s$  isomer ( $\text{S}_3$  ring with an out-of-plane oxygen atom bound to one of the sulfur atoms) is the global minimum on the potential energy surface [34]. B3LYP/cc-pVTZ calculations for this isomer done in the course of the present study yield  $A = 5984.7 \text{ MHz}$ ,  $B = 3353.0 \text{ MHz}$ ,  $C = 2401.5 \text{ MHz}$ ,  $\mu_a = 0.82 \text{ D}$ , and  $\mu_c = 1.45 \text{ D}$ . The low-lying  $c$ -type rotational transition  $1_{1,0} - 0_{0,0}$  at about  $9337.7 \text{ MHz}$  ( $= A + B$ ) falls in the band where our FTM spectrometer is most sensitive.

## Acknowledgements

This work was supported in part by NASA grant NAG5–9379 and NSF grant CHE–0353693. S. Thorwirth is grateful to the Alexander von Humboldt-Foundation for a Feodor Lynen research fellowship. P. Theulé would like to thank the Swiss National Science Foundation for a research fellowship.

<sup>4</sup> See the Cologne Database for Molecular Spectroscopy, CDMS [26], at <http://www.cdms.de> for an up-to-date list of astronomically detected molecules.

H. S. P. Müller acknowledges support by the Deutsche Forschungsgemeinschaft through SFB 494.

## References

- [1] D. J. Meschi, R. J. Myers, The Microwave Spectrum, Structure, and Dipole Moment of Disulfur Monoxide, *J. Mol. Spectrosc.* 3 (1959) 405–416.
- [2] R. L. Cook, G. Winnewisser, D. C. Lindsey, Centrifugal Distortion Constants of Disulfur Monoxide, *J. Mol. Spectrosc.* 46 (1973) 276–284.
- [3] E. Tiemann, J. Hoeft, F. J. Lovas, D. R. Johnson, Spectroscopic Studies of SO<sub>2</sub> Discharge System. I. Microwave-Spectrum and Structure of S<sub>2</sub>O, *J. Chem. Phys.* 60 (1974) 5000–5004.
- [4] J. Lindenmayer, The  $r_s$  Structure of Disulfur Monoxide - The Microwave-Spectrum of (S<sub>2</sub><sup>18</sup>O), *J. Mol. Spectrosc.* 116 (1986) 315–319.
- [5] J. Lindenmayer, H. Jones, The Diode-Laser Spectrum of the  $\nu_1$  Band of Disulfur Monoxide, *J. Mol. Spectrosc.* 112 (1985) 71–78.
- [6] J. Lindenmayer, H. D. Rudolph, H. Jones, The Equilibrium Structure of Disulfur Monoxide - Diode-Laser Spectroscopy of  $\nu_1$  and  $\nu_3$  of (S<sub>2</sub>O)-O-18 and  $\nu_3$  of S<sub>2</sub><sup>16</sup>O, *J. Mol. Spectrosc.* 119 (1986) 56–67.
- [7] T. Müller, P. H. Vaccaro, F. Pérez-Bernal, F. Iachello, The vibronically-resolved emission spectrum of disulfur monoxide (S<sub>2</sub>O): An algebraic calculation and quantitative interpretation of Franck-Condon transition intensities, *J. Chem. Phys.* 111 (1999) 5038–5055.
- [8] R. Steudel, Sulfur-Rich Oxides S<sub>n</sub>O and S<sub>n</sub>O<sub>2</sub> (n>1), *Top. Curr. Chem.* 231 (2003) 203–230.
- [9] M. C. McCarthy, S. Thorwirth, C. A. Gottlieb, P. Thaddeus, The Rotational Spectrum and Geometrical Structure of Thiozone, S<sub>3</sub>, *J. Am. Chem. Soc.* 126 (2004) 4096–4097.
- [10] M. C. McCarthy, S. Thorwirth, C. A. Gottlieb, P. Thaddeus, Tetrasulfur, S<sub>4</sub>: Rotational Spectrum, Interchange Tunneling, and Geometrical Structure, *J. Chem. Phys.* 121 (2004) 632–635.
- [11] S. Thorwirth, M. C. McCarthy, C. A. Gottlieb, P. Thaddeus, H. Gupta, J. F. Stanton, Rotational spectroscopy and equilibrium structures of S<sub>3</sub> and S<sub>4</sub>, *J. Chem. Phys.* 123 (2005) 054326.
- [12] M. C. McCarthy, M. J. Travers, A. Kovacs, C. A. Gottlieb, P. Thaddeus, Eight New Carbon Chain Molecules, *Astrophys. J. Suppl. Ser.* 113 (1997) 105–120.
- [13] M. C. McCarthy, W. Chen, M. J. Travers, P. Thaddeus, Microwave Spectra of 11 Polyynes Carbon Chains, *Astrophys. J. Suppl. Ser.* 129 (2000) 611–623.

- [14] M. E. Sanz, M. C. McCarthy, P. Thaddeus, Vibrational excitation and relaxation of five polyatomic molecules in an electrical discharge, *J. Chem. Phys.* 122 (2005) 194319.
- [15] C. A. Gottlieb, P. C. Myers, P. Thaddeus, Precise millimeter-wave laboratory frequencies for CS and C<sup>34</sup>S, *Astrophys. J.* 588 (2003) 655–661.
- [16] H. M. Pickett, The fitting and prediction of vibration-rotation spectra with spin interactions, *J. Mol. Spectrosc.* 148 (1991) 371–377.
- [17] G. Herzberg, *Molecular Spectra and Molecular Structure*, Vol. II, Krieger Publishing Co., Malabar, Florida, 1991.
- [18] H. D. Rudolph, Contribution to the systematics of  $r_0$ -derived molecular-structure determinations from rotational parameters, *Struct. Chem.* 2 (1991) 581–588.
- [19] H. S. P. Müller, M. C. L. Gerry, Microwave-Spectrum of Sulfuryl Chloride Fluoride, SO<sub>2</sub>CLF: Structure, Hyperfine Constants and Harmonic Force-Field, *J. Chem. Soc. Faraday Trans.* 90 (1994) 2601–2610.
- [20] M. J. Frisch, G. W. Trucks, H. B. Schlegel, et al., Gaussian 03, Revision B.04, Gaussian, Inc., Wallingford, CT (2003).
- [21] F. J. Lovas, E. Tiemann, D. R. Johnson, Spectroscopic studies of the SO<sub>2</sub> discharge system. II. Microwave spectrum of the SO dimer, *J. Chem. Phys.* 60 (1974) 5005–5010.
- [22] H. S. P. Müller, J. Farhoomand, E. A. Cohen, B. Brupbacher-Gatehouse, M. Schäfer, A. Bauder, G. Winnewisser, The rotational spectrum of SO<sub>2</sub> and the determination of the hyperfine constants and nuclear magnetic shielding tensors of <sup>33</sup>SO<sub>2</sub> and SO<sup>17</sup>O, *J. Mol. Spectrosc.* 201 (2000) 1–8.
- [23] W. Gordy, R. L. Cook, *Microwave Molecular Spectra*, 3rd Edition, Wiley, New York, 1984.
- [24] D. Christen, Least-Squares Refinement of Valence Force Constants Without Use of Molecular Symmetry, *J. Mol. Struct.* 48 (1978) 101–106.
- [25] T. Oka, Y. Morino, Calculation of Inertia Defect, Part II. Nonlinear Symmetric XY<sub>2</sub> Molecules, *J. Mol. Spectrosc.* 8 (1962) 9–21.
- [26] H. S. P. Müller, S. Thorwirth, D. A. Roth, G. Winnewisser, The Cologne Database for Molecular Spectroscopy, CDMS, *Astron. Astrophys.* 370 (2001) L49–L52.
- [27] C. Comito, P. Schilke, T. G. Phillips, D. C. Lis, F. Motte, D. Mehringer, A Molecular Line Survey of Orion KL in the 350 Micron Band, *Astrophys. J. Suppl. S.* 156 (2005) 127–167.
- [28] D. Bockelée-Morvan, J. Crovisier, Comets and Asteroids with FIRST, in: *ESA SP-460: The Promise of the Herschel Space Observatory*, 2001, pp. 279–286.

- [29] C. Y. Na, L. W. Esposito, Is disulfur monoxide a second absorber on Venus?, *Icarus* 125 (1997) 364–368.
- [30] M. Y. Zolotov, B. Fegley, Volcanic Origin of Disulfur Monoxide ( $S_2O$ ) on Io, *Icarus* 133 (1998) 293–297.
- [31] J. I. Moses, M. Y. Zolotov, B. Fegley, Photochemistry of a volcanically driven atmosphere on Io: Sulfur and oxygen species from a Pele-type eruption, *Icarus* 156 (2002) 76–106.
- [32] R. Steudel, Y. Steudel, The thermal decomposition of  $S_2O$  forming  $SO_2$ ,  $S_3$ ,  $S_4$  and  $S_5O$  - An ab initio MO study, *Eur. J. Inorg. Chem.* (2004) 3513–3521.
- [33] F. Cacace, G. de Petris, M. Rosi, A. Troiani,  $S_3O$ , a new sulfur oxide identified in the gas phase, *Chem. Commun.* (2001) 2086–2087.
- [34] M. W. Wong, R. Steudel, Structures of the trisulfur oxides  $S_3O$  and  $S_3O^+$ : branched rings, not open chains, *Chem. Commun.* (2005) 3712–3714.

Table 1

Experimental microwave transition frequencies of S<sub>2</sub>O in the ground vibrational and first excited vibrational states (in MHz) and residuals  $o - c$  (in kHz, global fit).

Transition	(0, 0, 0)	$o - c$	(1, 0, 0)	$o - c$	(0, 1, 0)	$o - c$	(0, 0, 1)	$o - c$
2 <sub>1,2</sub> - 3 <sub>0,3</sub>	7635.6394(20)	0.3	7331.3709(20)	0.8	8209.2989(20)	0.4	7790.6101(20)	-0.7
1 <sub>0,1</sub> - 0 <sub>0,0</sub>	9566.2535(20)	0.1	9544.6729(20)	-1.1	9560.6089(20)	-0.2	9523.0528(20)	0.3
5 <sub>0,5</sub> - 4 <sub>1,4</sub>	13258.9405(20)	-1.3	13522.6729(20)	1.0	12696.7339(30)	-0.1	13009.9395(20)	-0.6
1 <sub>1,1</sub> - 2 <sub>0,2</sub>	17728.9092(20)	1.3	17404.1709(20)	0.5	18303.6572(20)	0.7	17838.2598(20)	0.3
2 <sub>1,2</sub> - 1 <sub>1,1</sub>	18580.7120(20)	0.8	18536.0606(20)	0.8	18562.4414(20)	-0.5	18496.9815(20)	1.5
2 <sub>0,2</sub> - 1 <sub>0,1</sub>	19126.3106(20)	0.4	19083.0557(20)	-0.2	19114.9600(20)	0.3	19039.9707(20)	-0.6
2 <sub>1,1</sub> - 1 <sub>1,0</sub>	19684.4688(20)	0.2	19642.8037(20)	-0.8	19680.1709(20)	1.0	19595.3956(20)	0.0
3 <sub>1,3</sub> - 2 <sub>1,2</sub>	27867.1533(20)	1.2	27800.1163(20)	0.7	27839.7100(20)	0.1	27741.5938(20)	-0.6
3 <sub>0,3</sub> - 2 <sub>0,2</sub>	28673.9805(20)	0.5	28608.8594(20)	-0.6	28656.7998(20)	-0.1	28544.6299(20)	1.1
3 <sub>1,2</sub> - 2 <sub>1,1</sub>	29522.7061(20)	2.2	29460.1465(20)	-0.1	29516.2178(20)	0.6	29389.1348(20)	0.6
2 <sub>1,1</sub> - 2 <sub>0,2</sub>	37965.2618(20)	-1.6	37600.3555(20)	-0.2	38542.6973(20)	-1.3	37982.8711(20)	-0.1
4 <sub>0,4</sub> - 3 <sub>0,3</sub>	38203.1016(30)	1.4	—	—	—	—	—	—
3 <sub>1,2</sub> - 3 <sub>0,3</sub>	38813.9883(20)	0.9	—	—	—	—	—	—

Table 2

Vibrational satellites of S<sub>2</sub>O (in MHz) and residuals (in kHz, global fit).

Transition	(0, 2, 0)	<i>o</i> - <i>c</i>	(0, 3, 0)	<i>o</i> - <i>c</i>	(0, 4, 0)	<i>o</i> - <i>c</i>	(0, 5, 0)	<i>o</i> - <i>c</i>
1 <sub>0,1</sub> - 0 <sub>0,0</sub>	9554.7837(20)	0.3	9548.7769(20)	0.8	9542.5869(20)	0.0	9536.2154(20)	0.1
2 <sub>1,2</sub> - 1 <sub>1,1</sub>	18543.8360(20)	-0.8	18524.9034(20)	2.8	18505.6387(20)	0.3	18486.0557(20)	0.7
2 <sub>0,2</sub> - 1 <sub>0,1</sub>	19103.2500(20)	-0.2	19091.1797(20)	-1.1	19078.7500(20)	-1.1	19065.9610(20)	0.5
2 <sub>1,1</sub> - 1 <sub>1,0</sub>	19675.4814(20)	-0.4	19670.3985(20)	0.4	19664.9131(20)	0.5	19659.0196(20)	0.5
3 <sub>1,3</sub> - 2 <sub>1,2</sub>	27811.7657(20)	-0.3	27783.3272(20)	-0.5	27754.4004(20)	-2.1	27725.0000(30)	2.1
3 <sub>0,3</sub> - 2 <sub>0,2</sub>	28639.0889(20)	-0.8	28620.8477(20)	-1.0	28602.0762(20)	-0.1	28582.7725(20)	1.0
3 <sub>1,2</sub> - 2 <sub>1,1</sub>	—	—	—	—	29493.2285(30)	-0.1	29484.3584(20)	-0.2
4 <sub>1,4</sub> - 3 <sub>1,3</sub>	37074.9727(30)	3.2	37036.9883(30)	-0.3	36998.3613(30)	-1.3	36959.1016(30)	0.2
4 <sub>0,4</sub> - 3 <sub>0,3</sub>	38156.0215(20)	1.9	38131.4414(20)	-1.4	—	—	38080.2149(30)	2.1
Transition	(0, 6, 0)	<i>o</i> - <i>c</i>	(0, 7, 0)	<i>o</i> - <i>c</i>	(0, 8, 0)	<i>o</i> - <i>c</i>	(0, 1, 1)	<i>o</i> - <i>c</i>
1 <sub>0,1</sub> - 0 <sub>0,0</sub>	9529.6607(20)	-0.4	—	—	9516.0034(20)	-0.1	9517.4732(20)	0.7
2 <sub>1,2</sub> - 1 <sub>1,1</sub>	—	—	—	—	—	—	18478.7461(20)	-0.2
2 <sub>0,2</sub> - 1 <sub>0,1</sub>	19052.8086(20)	0.3	19039.2930(20)	-0.9	19025.4180(20)	1.3	19028.7461(20)	-1.3
2 <sub>1,1</sub> - 1 <sub>1,0</sub>	—	—	—	—	—	—	19591.3193(20)	0.3
3 <sub>1,3</sub> - 2 <sub>1,2</sub>	—	—	—	—	—	—	27714.2022(20)	-1.8
3 <sub>0,3</sub> - 2 <sub>0,2</sub>	28562.9336(20)	-0.1	28542.5606(20)	-1.4	—	—	28527.6328(20)	-0.1
3 <sub>1,2</sub> - 2 <sub>1,1</sub>	—	—	—	—	—	—	29382.9805(30)	1.3
Transition	(0, 2, 1)	<i>o</i> - <i>c</i>	(0, 3, 1)	<i>o</i> - <i>c</i>	(0, 4, 1)	<i>o</i> - <i>c</i>		
1 <sub>0,1</sub> - 0 <sub>0,0</sub>	9511.7027(20)	-0.6	9505.7456(20)	1.1	9499.5962(20)	0.5		
2 <sub>1,2</sub> - 1 <sub>1,1</sub>	18460.1621(20)	-0.2	18441.2344(20)	1.3	18421.9620(20)	-1.5		
2 <sub>0,2</sub> - 1 <sub>0,1</sub>	19017.1495(20)	1.1	19005.1748(20)	1.0	18992.8213(20)	-1.6		
2 <sub>1,1</sub> - 1 <sub>1,0</sub>	19586.8340(20)	-1.5	19581.9365(30)	-2.2	—	—		
3 <sub>0,3</sub> - 2 <sub>0,2</sub>	28510.0830(20)	-0.1	28491.9805(20)	1.7	28473.3203(30)	1.2		

Table 3: Experimental millimeter- and submillimeter-wave transition frequencies of S<sub>2</sub>O in the ground vibrational state and residuals (in MHz, global fit).

Transition	Frequency	$o - c$
32 <sub>2,30</sub> – 32 <sub>1,31</sub>	163895.727(20)	0.007
54 <sub>11,44</sub> – 55 <sub>10,45</sub>	245248.439(20)	–0.005
54 <sub>11,43</sub> – 55 <sub>10,46</sub>	245248.439(20)	–0.005
69 <sub>13,57</sub> – 70 <sub>12,58</sub>	246507.467(40)	0.016
69 <sub>13,56</sub> – 70 <sub>12,59</sub>	246507.467(40)	0.016
26 <sub>10,16</sub> – 25 <sub>10,15</sub>	248963.124(20)	0.012
26 <sub>10,17</sub> – 25 <sub>10,16</sub>	248963.124(20)	0.012
26 <sub>11,15</sub> – 25 <sub>11,14</sub>	248965.204(20)	0.007
26 <sub>11,16</sub> – 25 <sub>11,15</sub>	248965.204(20)	0.007
26 <sub>9,17</sub> – 25 <sub>9,16</sub>	248975.397(20)	–0.012
26 <sub>9,18</sub> – 25 <sub>9,17</sub>	248975.397(20)	–0.012
26 <sub>12,14</sub> – 25 <sub>12,13</sub>	248977.922(20)	–0.013
26 <sub>12,15</sub> – 25 <sub>12,14</sub>	248977.922(20)	–0.013
26 <sub>13,13</sub> – 25 <sub>13,12</sub>	248998.980(20)	0.010
26 <sub>13,14</sub> – 25 <sub>13,13</sub>	248998.980(20)	0.010
26 <sub>8,19</sub> – 25 <sub>8,18</sub>	249008.334(20)	0.005
26 <sub>8,18</sub> – 25 <sub>8,17</sub>	249008.334(20)	0.005
26 <sub>14,12</sub> – 25 <sub>14,11</sub>	249026.730(20)	–0.013
26 <sub>14,13</sub> – 25 <sub>14,12</sub>	249026.730(20)	–0.013
26 <sub>15,11</sub> – 25 <sub>15,10</sub>	249060.188(20)	0.011
26 <sub>15,12</sub> – 25 <sub>15,11</sub>	249060.188(20)	0.011
26 <sub>7,20</sub> – 25 <sub>7,19</sub>	249073.052(20)	–0.004
26 <sub>7,19</sub> – 25 <sub>7,18</sub>	249073.052(20)	–0.004
26 <sub>17,9</sub> – 25 <sub>17,8</sub>	249141.141(20)	0.007
26 <sub>17,10</sub> – 25 <sub>17,9</sub>	249141.141(20)	0.007
26 <sub>18,8</sub> – 25 <sub>18,7</sub>	249187.652(20)	0.010
26 <sub>18,9</sub> – 25 <sub>18,8</sub>	249187.652(20)	0.010
26 <sub>19,7</sub> – 25 <sub>19,6</sub>	249237.685(20)	0.011
26 <sub>19,8</sub> – 25 <sub>19,7</sub>	249237.685(20)	0.011
26 <sub>3,24</sub> – 25 <sub>3,23</sub>	249242.588(20)	–0.020
26 <sub>20,6</sub> – 25 <sub>20,5</sub>	249290.949(20)	0.004
26 <sub>20,7</sub> – 25 <sub>20,6</sub>	249290.949(20)	0.004
26 <sub>21,5</sub> – 25 <sub>21,4</sub>	249347.215(20)	0.000
26 <sub>21,6</sub> – 25 <sub>21,5</sub>	249347.215(20)	0.000
26 <sub>5,22</sub> – 25 <sub>5,21</sub>	249403.523(20)	–0.005
26 <sub>22,4</sub> – 25 <sub>22,3</sub>	249406.269(20)	–0.010
26 <sub>22,5</sub> – 25 <sub>22,4</sub>	249406.269(20)	–0.010
27 <sub>1,27</sub> – 26 <sub>0,26</sub>	250252.926(20)	0.000
38 <sub>9,30</sub> – 39 <sub>8,31</sub>	253407.272(20)	–0.037
38 <sub>9,29</sub> – 39 <sub>8,32</sub>	253407.272(20)	–0.037
53 <sub>11,43</sub> – 54 <sub>10,44</sub>	255059.168(20)	–0.013
53 <sub>11,42</sub> – 54 <sub>10,45</sub>	255059.168(20)	–0.013

Table 3 – *Continued*

Transition	Frequency	$o - c$
7 <sub>5,3</sub> – 8 <sub>4,4</sub>	257160.680(20)	0.006
7 <sub>5,2</sub> – 8 <sub>4,5</sub>	257160.680(20)	0.006
22 <sub>4,19</sub> – 22 <sub>3,20</sub>	259190.384(20)	0.005
45 <sub>10,36</sub> – 46 <sub>9,37</sub>	259193.191(20)	0.018
45 <sub>10,35</sub> – 46 <sub>9,38</sub>	259193.191(20)	0.018
11 <sub>4,7</sub> – 11 <sub>3,8</sub>	259415.944(20)	0.001
13 <sub>4,10</sub> – 13 <sub>3,11</sub>	259419.832(20)	–0.009
11 <sub>4,8</sub> – 11 <sub>3,9</sub>	259542.283(20)	–0.013
9 <sub>4,6</sub> – 9 <sub>3,7</sub>	259629.447(20)	–0.025
25 <sub>4,22</sub> – 25 <sub>3,23</sub>	259932.009(20)	–0.014
26 <sub>4,23</sub> – 26 <sub>3,24</sub>	260380.413(20)	–0.009
60 <sub>12,49</sub> – 61 <sub>11,50</sub>	260621.874(20)	–0.005
60 <sub>12,48</sub> – 61 <sub>11,51</sub>	260621.874(20)	–0.005
27 <sub>4,24</sub> – 27 <sub>3,25</sub>	260955.616(20)	0.004
28 <sub>4,25</sub> – 28 <sub>3,26</sub>	261673.852(20)	–0.005
29 <sub>4,26</sub> – 29 <sub>3,27</sub>	262551.498(20)	0.001
37 <sub>9,29</sub> – 38 <sub>8,30</sub>	263166.319(20)	0.015
37 <sub>9,28</sub> – 38 <sub>8,31</sub>	263166.319(20)	0.015
36 <sub>3,34</sub> – 36 <sub>2,35</sub>	263474.829(20)	–0.001
30 <sub>4,27</sub> – 30 <sub>3,28</sub>	263604.730(20)	–0.011
31 <sub>4,28</sub> – 31 <sub>3,29</sub>	264849.472(20)	0.005
32 <sub>4,29</sub> – 32 <sub>3,30</sub>	266301.037(20)	0.015
42 <sub>12,30</sub> – 43 <sub>11,33</sub>	435224.649(30)	–0.007
42 <sub>12,31</sub> – 43 <sub>11,32</sub>	435224.649(30)	–0.007
47 <sub>1,46</sub> – 46 <sub>2,45</sub>	435276.512(30)	–0.005
41 <sub>3,39</sub> – 40 <sub>2,38</sub>	436318.613(30)	–0.031
48 <sub>0,48</sub> – 47 <sub>1,47</sub>	436656.451(30)	–0.018
48 <sub>1,48</sub> – 47 <sub>1,47</sub>	436690.197(30)	0.005
48 <sub>0,48</sub> – 47 <sub>0,47</sub>	436698.000(30)	0.002
48 <sub>1,48</sub> – 47 <sub>0,47</sub>	436731.731(30)	0.009
34 <sub>11,23</sub> – 35 <sub>10,26</sub>	439224.944(30)	0.005
34 <sub>11,24</sub> – 35 <sub>10,25</sub>	439224.944(30)	0.005
46 <sub>14,32</sub> – 45 <sub>14,31</sub>	440432.445(50)	0.021
46 <sub>14,33</sub> – 45 <sub>14,32</sub>	440432.445(50)	0.021
46 <sub>13,33</sub> – 45 <sub>13,32</sub>	440438.270(50)	0.053
46 <sub>13,34</sub> – 45 <sub>13,33</sub>	440438.270(50)	0.053
46 <sub>15,31</sub> – 45 <sub>15,30</sub>	440447.360(50)	–0.005
46 <sub>15,32</sub> – 45 <sub>15,31</sub>	440447.360(50)	–0.005
46 <sub>16,30</sub> – 45 <sub>16,29</sub>	440479.039(30)	0.000
46 <sub>16,31</sub> – 45 <sub>16,30</sub>	440479.039(30)	0.000
46 <sub>17,29</sub> – 45 <sub>17,28</sub>	440524.569(30)	0.011
46 <sub>17,30</sub> – 45 <sub>17,29</sub>	440524.569(30)	0.011
46 <sub>11,35</sub> – 45 <sub>11,34</sub>	440537.645(30)	0.003



Table 3 – *Continued*

Transition	Frequency	$o - c$
46 <sub>11,36</sub> – 45 <sub>11,35</sub>	440537.645(30)	0.003
46 <sub>18,28</sub> – 45 <sub>18,27</sub>	440581.778(30)	–0.007
46 <sub>18,29</sub> – 45 <sub>18,28</sub>	440581.778(30)	–0.007
46 <sub>10,37</sub> – 45 <sub>10,36</sub>	440652.798(30)	–0.001
46 <sub>10,36</sub> – 45 <sub>10,35</sub>	440652.798(30)	–0.001
42 <sub>3,40</sub> – 41 <sub>2,39</sub>	440744.975(30)	–0.011
46 <sub>9,38</sub> – 45 <sub>9,37</sub>	440837.070(30)	–0.019
46 <sub>9,37</sub> – 45 <sub>9,36</sub>	440837.070(30)	–0.019
46 <sub>7,40</sub> – 45 <sub>7,39</sub>	441583.748(30)	0.024
46 <sub>7,39</sub> – 45 <sub>7,38</sub>	441600.318(30)	–0.007
46 <sub>6,41</sub> – 45 <sub>6,40</sub>	442259.387(30)	0.001
46 <sub>6,40</sub> – 45 <sub>6,39</sub>	442510.077(30)	–0.003
46 <sub>5,42</sub> – 45 <sub>5,41</sub>	442756.927(30)	–0.003
58 <sub>3,56</sub> – 58 <sub>2,57</sub>	443223.450(30)	0.011
48 <sub>1,47</sub> – 47 <sub>2,46</sub>	444512.230(30)	0.001
46 <sub>5,41</sub> – 45 <sub>5,40</sub>	445050.663(30)	–0.001
24 <sub>3,21</sub> – 23 <sub>2,22</sub>	445225.357(30)	–0.007
43 <sub>3,41</sub> – 42 <sub>2,40</sub>	445469.289(20)	–0.004
53 <sub>3,50</sub> – 52 <sub>4,49</sub>	445528.790(30)	–0.002
49 <sub>0,49</sub> – 48 <sub>1,48</sub>	445642.747(30)	–0.002
49 <sub>1,49</sub> – 48 <sub>1,48</sub>	445670.117(30)	–0.000
49 <sub>0,49</sub> – 48 <sub>0,48</sub>	445676.473(30)	0.001
49 <sub>1,49</sub> – 48 <sub>0,48</sub>	445703.833(30)	–0.008
56 <sub>14,42</sub> – 57 <sub>13,45</sub>	445876.513(30)	–0.030
56 <sub>14,43</sub> – 57 <sub>13,44</sub>	445876.513(30)	–0.030
69 <sub>5,65</sub> – 69 <sub>4,66</sub>	446143.328(30)	0.012
18 <sub>9,9</sub> – 19 <sub>8,12</sub>	446475.954(30)	0.004
18 <sub>9,10</sub> – 19 <sub>8,11</sub>	446475.954(30)	0.004
48 <sub>2,47</sub> – 47 <sub>1,46</sub>	447206.382(30)	0.018
20 <sub>4,17</sub> – 19 <sub>3,16</sub>	447820.218(30)	–0.027
33 <sub>11,22</sub> – 34 <sub>10,25</sub>	448834.908(30)	0.005
33 <sub>11,23</sub> – 34 <sub>10,24</sub>	448834.908(30)	0.005
44 <sub>3,42</sub> – 43 <sub>2,41</sub>	450503.258(30)	0.068
59 <sub>3,57</sub> – 59 <sub>2,58</sub>	452290.555(30)	–0.005
54 <sub>1,53</sub> – 54 <sub>0,54</sub>	452394.733(30)	–0.002
25 <sub>10,15</sub> – 26 <sub>9,18</sub>	452578.667(30)	0.000
25 <sub>10,16</sub> – 26 <sub>9,17</sub>	452578.667(30)	0.000
70 <sub>5,66</sub> – 70 <sub>4,67</sub>	453998.820(30)	0.040
50 <sub>0,50</sub> – 49 <sub>1,49</sub>	454626.326(30)	0.002
50 <sub>1,50</sub> – 49 <sub>1,49</sub>	454648.520(30)	–0.002
50 <sub>0,50</sub> – 49 <sub>0,49</sub>	454653.680(30)	–0.012
66 <sub>3,63</sub> – 66 <sub>2,64</sub>	455409.466(30)	0.006
55 <sub>14,41</sub> – 56 <sub>13,44</sub>	455493.311(50)	0.087

Table 3 – *Continued*

Transition	Frequency	$o - c$
55 <sub>14,42</sub> – 56 <sub>13,43</sub>	455493.311(50)	0.087
17 <sub>9,8</sub> – 18 <sub>8,11</sub>	456057.253(30)	0.007
17 <sub>9,9</sub> – 18 <sub>8,10</sub>	456057.253(30)	0.007
65 <sub>4,62</sub> – 65 <sub>3,63</sub>	457306.946(30)	–0.048
13 <sub>5,9</sub> – 12 <sub>4,8</sub>	458102.134(30)	–0.006
13 <sub>5,8</sub> – 12 <sub>4,9</sub>	458105.336(30)	–0.035
55 <sub>7,48</sub> – 55 <sub>6,49</sub>	458436.121(30)	0.011
32 <sub>11,21</sub> – 33 <sub>10,24</sub>	458439.595(30)	0.012
32 <sub>11,22</sub> – 33 <sub>10,23</sub>	458439.595(30)	0.012
60 <sub>2,58</sub> – 60 <sub>1,59</sub>	458894.946(30)	0.025
66 <sub>7,60</sub> – 66 <sub>6,61</sub>	459783.673(30)	–0.015
67 <sub>7,61</sub> – 67 <sub>6,62</sub>	459854.330(30)	–0.001
65 <sub>7,59</sub> – 65 <sub>6,60</sub>	459869.325(30)	0.045
25 <sub>3,22</sub> – 24 <sub>2,23</sub>	460473.047(30)	–0.004
69 <sub>7,63</sub> – 69 <sub>6,64</sub>	460527.746(30)	–0.009
21 <sub>4,17</sub> – 20 <sub>3,18</sub>	460775.735(30)	0.028
54 <sub>3,51</sub> – 53 <sub>4,50</sub>	460845.741(30)	–0.006
62 <sub>7,56</sub> – 62 <sub>6,57</sub>	460905.331(30)	–0.015
48 <sub>7,42</sub> – 47 <sub>7,41</sub>	460907.816(30)	–0.025
48 <sub>7,41</sub> – 47 <sub>7,40</sub>	460936.258(30)	0.014
60 <sub>3,58</sub> – 60 <sub>2,59</sub>	461375.540(30)	0.002
61 <sub>7,55</sub> – 61 <sub>6,56</sub>	461459.107(30)	–0.000
55 <sub>1,54</sub> – 55 <sub>0,55</sub>	461541.835(30)	–0.005
55 <sub>2,54</sub> – 55 <sub>1,55</sub>	461869.046(30)	–0.004
71 <sub>7,65</sub> – 71 <sub>6,66</sub>	462013.775(30)	–0.017
71 <sub>5,67</sub> – 71 <sub>4,68</sub>	462023.503(30)	–0.028
48 <sub>5,44</sub> – 47 <sub>5,43</sub>	462036.559(30)	–0.007
48 <sub>6,42</sub> – 47 <sub>6,41</sub>	462036.559(30)	–0.007
24 <sub>10,14</sub> – 25 <sub>9,17</sub>	462170.058(30)	0.030
24 <sub>10,15</sub> – 25 <sub>9,16</sub>	462170.058(30)	0.030
59 <sub>7,53</sub> – 59 <sub>6,54</sub>	462791.921(30)	0.010
50 <sub>1,49</sub> – 49 <sub>2,48</sub>	462862.236(30)	–0.017
58 <sub>7,52</sub> – 58 <sub>6,53</sub>	463544.207(30)	0.011
51 <sub>0,51</sub> – 50 <sub>1,50</sub>	463607.388(30)	–0.016
51 <sub>1,51</sub> – 50 <sub>1,50</sub>	463625.391(30)	–0.008
51 <sub>0,51</sub> – 50 <sub>0,50</sub>	463629.596(30)	–0.006
51 <sub>1,51</sub> – 50 <sub>0,50</sub>	463647.618(30)	0.021
57 <sub>7,51</sub> – 57 <sub>6,52</sub>	464337.278(30)	0.015
73 <sub>7,67</sub> – 73 <sub>6,68</sub>	464428.885(30)	0.018
6 <sub>6,0</sub> – 5 <sub>5,1</sub>	465075.004(30)	–0.006
6 <sub>6,1</sub> – 5 <sub>5,0</sub>	465075.004(30)	–0.006
56 <sub>7,50</sub> – 56 <sub>6,51</sub>	465159.858(30)	–0.021
16 <sub>9,7</sub> – 17 <sub>8,10</sub>	465635.514(30)	0.016

Table 3 – *Continued*

Transition	Frequency	$o - c$
$16_{9,8} - 17_{8,9}$	465635.514(30)	0.016
$55_{7,49} - 55_{6,50}$	466001.762(30)	0.002
$74_{7,68} - 74_{6,69}$	466017.807(30)	-0.011
$51_{7,44} - 51_{6,45}$	466036.076(30)	-0.013
$54_{7,48} - 54_{6,49}$	466853.576(30)	-0.021
$50_{7,43} - 50_{6,44}$	467509.871(30)	0.009
$31_{11,20} - 32_{10,23}$	468039.336(30)	-0.012
$31_{11,21} - 32_{10,22}$	468039.336(30)	-0.012
$52_{7,46} - 52_{6,47}$	468554.783(30)	-0.011
$49_{7,42} - 49_{6,43}$	468845.854(30)	-0.003
$51_{7,45} - 51_{6,46}$	469390.399(30)	0.013
$76_{7,70} - 76_{6,71}$	470015.640(200)	-0.040
$49_{8,42} - 48_{8,41}$	470017.797(100)	0.029
$49_{8,41} - 48_{8,40}$	470019.692(100)	-0.012

Table 4  
Molecular Parameters of S<sub>2</sub>O (in MHz).

Fit 1 <sup>a</sup>			Fit 2 <sup>b</sup>						
Parameter	Value	Parameter	Value	Parameter	Value				
$A_0$	41915.42761(86)	$A_e$	41829.107(91)	$\alpha_1^A$	-378.0507(16)	$\alpha_2^A$	546.08(24)	$\alpha_3^A$	0.0892(16)
$B_0$	5059.09997(13)	$B_e$	5075.23382(63)	$\alpha_1^B$	-10.04276(25)	$\alpha_2^B$	0.7354(11)	$\alpha_3^B$	-22.97714(53)
$C_0$	4507.16100(16)	$C_e$	4526.18911(71)	$\alpha_1^C$	-11.53660(36)	$\alpha_2^C$	-6.2348(11)	$\alpha_3^C$	-20.25897(61)
$\Delta_{J_0} \times 10^3$	1.891474(81)	$\Delta_{J_e} \times 10^3$	1.8804(12)	$\alpha_1^{\Delta J} \times 10^6$	15.14(50)	$\beta_{22}^{\Delta J}$	9.04(12)	$\alpha_3^{\Delta J} \times 10^6$	0.87(58)
$\Delta_{JK_0} \times 10^3$	-32.1264(18)	$\Delta_{JK_e} \times 10^3$	-31.308(26)	$\alpha_1^{\Delta K} \times 10^3$	-15.32(28)	$\beta_{22}^{\Delta K} \times 10^3$	-48.61(37)	$\alpha_3^{\Delta K} \times 10^3$	-0.435(30)
$\Delta_{K_0}$	1.200100(26)	$\Delta_{K_e}$	1.15927(78)	$\alpha_1^{\delta J} \times 10^6$	4.54(47)	$\beta_{22}^{\delta J} \times 10^3$	-39.82(36)	$\alpha_3^{\delta J} \times 10^3$	12.32(12)
$\delta_{J_0} \times 10^3$	0.345616(64)	$\delta_{J_e} \times 10^3$	0.34371(38)	$E_1$	34969400.6(20)	$\gamma_{222}^B \times 10^3$	-0.490(38)	$\alpha_3^{\delta J} \times 10^6$	-0.74(59)
$\delta_{K_0} \times 10^3$	12.3046(66)	$\delta_{K_e} \times 10^3$	10.94(15)			$\gamma_{222}^C \times 10^3$	0.436(38)	$E_3$	20359987.6(30)
$\Phi_{J_0} \times 10^9$	1.036(19)	$\Phi_{J_e} \times 10^9$	1.036(19)			$\beta_{23}^B \times 10^3$	83.63(88)		
$\Phi_{JK_0} \times 10^9$	47.0(16)	$\Phi_{JK_e} \times 10^9$	47.0(16)			$\beta_{23}^C \times 10^3$	-11.27(80)		
$\Phi_{KJ_0} \times 10^6$	-4.874(11)	$\Phi_{KJ_e} \times 10^6$	-4.874(11)			$\gamma_{223}^B \times 10^3$	-2.40(22)		
$\Phi_{K_0} \times 10^3$	0.12239(25)	$\Phi_{K_e} \times 10^3$	0.12241(25)			$\gamma_{223}^C \times 10^3$	-1.58(18)		
$\phi_{J_0} \times 10^9$	0.568(25)	$\phi_{J_e} \times 10^9$	0.566(25)			$\alpha_2^{\Delta J} \times 10^6$	6.1(22)		
$\phi_{JK_0} \times 10^9$	18.4(24)	$\phi_{JK_e} \times 10^9$	18.4(24)			$\alpha_2^{\Delta K} \times 10^3$	-1.202(43)		
$\phi_{K_0} \times 10^6$	5.31(12)	$\phi_{K_e} \times 10^6$	5.31(12)			$\alpha_2^{\delta K} \times 10^3$	80.7(15)		
$L_{JK_0} \times 10^{12}$	-0.38(11)	$L_{JK_e} \times 10^{12}$	-0.38(11)			$\alpha_2^{\delta K} \times 10^3$	2.73(30)		
$L_{JK_0} \times 10^{12}$	-5.5(16)	$L_{JK_e} \times 10^{12}$	-5.5(16)			$\beta_{22}^{\Delta K} \times 10^3$	8.0 <sup>c</sup>		
$L_{KKJ_0} \times 10^9$	0.687(15)	$L_{KKJ_e} \times 10^9$	0.687(15)						
$L_{K_0} \times 10^9$	-16.36(66)	$L_{K_e} \times 10^9$	-16.41(66)						
$l_{J_0} \times 10^{15}$	-6.7(29)	$l_{J_e} \times 10^{15}$	-6.5(29)						

<sup>a</sup> Fit to the rotational and rotation-vibration data of the (0, 0, 0), (1, 0, 0), and (0, 0, 1) states (see Sec. 3.1).

<sup>b</sup> Global fit to all available rotational and rotation-vibration data (see Sec. 3.1).

<sup>c</sup> Constrained. Based on the ratios  $A_e/\alpha_2^A \approx 75$ ,  $\alpha_2^A/\beta_{22}^A \approx 60$ , and  $\Delta_{Ke}/\alpha_2^{\Delta K} \approx 14$  it was assumed that  $\alpha_2^{\Delta K}/\beta_{22}^{\Delta K}$  is of order 10.

Table 5  
 Experimental microwave transition frequencies of  $^{34}\text{SSO}$  and  $\text{S}^{34}\text{SO}$  (in MHz) and residuals (in kHz).

Transition	$^{34}\text{SSO}$		$\text{S}^{34}\text{SO}$	
	Frequency	$o - c$	Frequency	$o - c$
$2_{1,2} - 3_{0,3}$	8496.5327(20)	1.3	—	
$1_{0,1} - 0_{0,0}$	9281.2915(20)	-1.2	9506.9292(20)	0.4
$2_{1,2} - 1_{1,1}$	18040.8770(20)	-0.4	18451.9443(30)	-0.8
$1_{1,1} - 2_{0,2}$	18277.3496(20)	-0.4	16594.2647(30)	0.4
$2_{0,2} - 1_{0,1}$	18557.0381(20)	-0.5	19007.2129(20)	0.3
$2_{1,1} - 1_{1,0}$	19084.4541(30)	-0.1	19575.9160(20)	-0.4
$3_{1,3} - 2_{1,2}$	27057.8077(20)	0.2	27673.7266(30)	-0.5
$3_{0,3} - 2_{0,2}$	27821.6973(20)	1.3	28494.2129(20)	-0.6
$3_{1,2} - 2_{1,1}$	28623.0997(20)	1.2	29359.5928(30)	-1.5
$4_{1,4} - 3_{1,3}$	36070.5801(40)	1.7	36890.5469(40)	-1.8
$4_{0,4} - 3_{0,3}$	37069.7461(20)	0.5	37961.3281(20)	1.5
$1_{1,0} - 1_{0,1}$	37356.1856(20)	1.0	36163.4707(20)	-0.2
$2_{1,1} - 2_{0,2}$	37883.5977(20)	-2.5	36732.1739(20)	-0.8
$4_{1,3} - 3_{1,2}$	38157.3906(30)	-2.5	38774.2950(40)	-2.5
$3_{1,2} - 3_{0,3}$	38685.0039(30)	1.3	37597.5567(20)	1.2

Table 6  
 Millimeter wave transition frequencies of  $^{34}\text{SSO}$  and  $\text{S}^{34}\text{SO}$  and residuals (in MHz).

$^{34}\text{SSO}$			$\text{S}^{34}\text{SO}$		
Transition	Frequency	$o - c$	Transition	Frequency	$o - c$
10 <sub>1,10</sub> – 9 <sub>1,9</sub>	89992.867(20)	–0.018	16 <sub>2,14</sub> – 16 <sub>1,15</sub>	90039.597(20)	0.002
10 <sub>6,4</sub> – 9 <sub>6,3</sub>	92863.248(30)	–0.024	15 <sub>2,13</sub> – 15 <sub>1,14</sub>	90201.093(20)	0.010
10 <sub>6,5</sub> – 9 <sub>6,4</sub>	92863.248(30)	–0.024	17 <sub>2,15</sub> – 17 <sub>1,16</sub>	90316.885(40)	–0.042
10 <sub>7,3</sub> – 9 <sub>7,2</sub>	92864.074(30)	0.037	14 <sub>2,12</sub> – 14 <sub>1,13</sub>	90752.799(20)	0.009
10 <sub>7,4</sub> – 9 <sub>7,3</sub>	92864.074(30)	0.037	18 <sub>2,16</sub> – 18 <sub>1,17</sub>	91077.117(20)	–0.002
10 <sub>5,6</sub> – 9 <sub>5,5</sub>	92868.579(30)	–0.002	12 <sub>0,12</sub> – 11 <sub>1,11</sub>	91425.196(20)	–0.002
10 <sub>5,5</sub> – 9 <sub>5,4</sub>	92868.579(30)	–0.002	13 <sub>2,11</sub> – 13 <sub>1,12</sub>	91641.535(20)	0.000
10 <sub>8,2</sub> – 9 <sub>8,1</sub>	92868.579(30)	–0.002	10 <sub>1,10</sub> – 9 <sub>1,9</sub>	92008.886(20)	0.006
10 <sub>8,3</sub> – 9 <sub>8,2</sub>	92868.579(30)	–0.002	19 <sub>2,17</sub> – 19 <sub>1,18</sub>	92359.944(20)	0.004
10 <sub>9,1</sub> – 9 <sub>9,0</sub>	92875.605(20)	–0.004	12 <sub>2,10</sub> – 12 <sub>1,11</sub>	92809.946(20)	–0.008
10 <sub>9,2</sub> – 9 <sub>9,1</sub>	92875.605(20)	–0.004	10 <sub>0,10</sub> – 9 <sub>0,9</sub>	94008.558(20)	–0.002
10 <sub>4,7</sub> – 9 <sub>4,6</sub>	92886.061(30)	–0.004	11 <sub>2,9</sub> – 11 <sub>1,10</sub>	94197.380(20)	–0.006
10 <sub>4,6</sub> – 9 <sub>4,5</sub>	92886.061(30)	–0.004	20 <sub>2,18</sub> – 20 <sub>1,19</sub>	94201.257(20)	–0.002
10 <sub>3,8</sub> – 9 <sub>3,7</sub>	92921.212(20)	0.010	10 <sub>2,9</sub> – 9 <sub>2,8</sub>	94897.930(20)	0.000
10 <sub>3,7</sub> – 9 <sub>3,6</sub>	92949.775(20)	–0.020	10 <sub>7,3</sub> – 9 <sub>7,2</sub>	95124.426(40)	0.029
17 <sub>2,15</sub> – 17 <sub>1,16</sub>	93100.348(20)	0.003	10 <sub>7,4</sub> – 9 <sub>7,3</sub>	95124.426(40)	0.029
16 <sub>2,14</sub> – 16 <sub>1,15</sub>	93212.153(20)	0.009	10 <sub>6,4</sub> – 9 <sub>6,3</sub>	95125.417(40)	0.019
18 <sub>2,16</sub> – 18 <sub>1,17</sub>	93399.535(20)	–0.008	10 <sub>6,5</sub> – 9 <sub>6,4</sub>	95125.417(40)	0.019
10 <sub>2,8</sub> – 9 <sub>2,7</sub>	93553.021(30)	–0.005	10 <sub>8,2</sub> – 9 <sub>8,1</sub>	95127.550(40)	–0.022
15 <sub>2,13</sub> – 15 <sub>1,14</sub>	93692.658(20)	–0.006	10 <sub>8,3</sub> – 9 <sub>8,2</sub>	95127.550(40)	–0.022
19 <sub>2,17</sub> – 19 <sub>1,18</sub>	94148.228(20)	0.006	10 <sub>5,6</sub> – 9 <sub>5,5</sub>	95133.457(30)	0.005
14 <sub>2,12</sub> – 14 <sub>1,13</sub>	94495.780(20)	–0.001	10 <sub>5,5</sub> – 9 <sub>5,4</sub>	95133.457(30)	0.005
7 <sub>1,7</sub> – 6 <sub>0,6</sub>	94992.784(20)	–0.003	10 <sub>9,1</sub> – 9 <sub>9,0</sub>	95133.457(30)	0.005
10 <sub>1,9</sub> – 9 <sub>1,8</sub>	95179.747(20)	–0.002	10 <sub>9,2</sub> – 9 <sub>9,1</sub>	95133.457(30)	0.005
20 <sub>2,18</sub> – 20 <sub>1,19</sub>	95381.318(40)	0.007	10 <sub>4,7</sub> – 9 <sub>4,6</sub>	95155.654(30)	–0.055
13 <sub>2,11</sub> – 13 <sub>1,12</sub>	95571.798(20)	0.014	10 <sub>4,6</sub> – 9 <sub>4,5</sub>	95155.654(30)	–0.055
12 <sub>2,10</sub> – 12 <sub>1,11</sub>	96867.987(20)	–0.001	10 <sub>3,8</sub> – 9 <sub>3,7</sub>	95197.044(20)	0.016
21 <sub>2,19</sub> – 21 <sub>1,20</sub>	97130.472(20)	–0.004	10 <sub>3,7</sub> – 9 <sub>3,6</sub>	95235.157(30)	–0.014
13 <sub>0,13</sub> – 12 <sub>1,12</sub>	97920.594(20)	0.013	10 <sub>2,8</sub> – 10 <sub>1,9</sub>	95741.169(20)	–0.015
11 <sub>2,9</sub> – 11 <sub>1,10</sub>	98329.676(20)	–0.013	10 <sub>2,8</sub> – 9 <sub>2,7</sub>	95950.783(40)	–0.024
			21 <sub>2,19</sub> – 21 <sub>1,20</sub>	96633.287(20)	0.001
			9 <sub>2,7</sub> – 9 <sub>1,8</sub>	97378.341(20)	0.017
			10 <sub>1,9</sub> – 9 <sub>1,8</sub>	97587.953(20)	0.005

Table 7  
 Rotational Constants of  $^{34}\text{SSO}$  and  $\text{S}^{34}\text{SO}$  (in MHz)<sup>a</sup>.

Parameter	$^{34}\text{SSO}$	$\text{S}^{34}\text{SO}$
$A$	41737.0575 (23)	40637.0055(25)
$B$	4901.57321 (50)	5034.49061(54)
$C$	4379.72661 ( 51)	4472.44565(54)
$\Delta_J \times 10^3$	1.7815(23)	1.8552(24)
$\Delta_{JK} \times 10^3$	-30.795(45)	-29.401(65)
$\Delta_K$	1.1827(20)	1.1224(18)
$\delta_J \times 10^3$	0.31585(78)	0.34428(75)
$\delta_K \times 10^3$	12.03(20)	12.07(22)
$\Phi_{KJ} \times 10^6$	-4.97 (56)	-4.35(116)

<sup>a</sup> Higher-order centrifugal distortion constants were constrained to those of the main species (Table 4, Fit 1).

Table 8  
 Experimental transition frequencies of  $^{33}\text{SSO}$  and  $\text{S}^{33}\text{SO}$  (in MHz) and residuals (in kHz).

Transition		$^{33}\text{SSO}$		$\text{S}^{33}\text{SO}$	
$J'_{K'_a, K'_c} - J''_{K''_a, K''_c}$	$F' - F''$	Frequency	$o - c$	Frequency	$o - c$
$1_{0,1} - 0_{0,0}$	1.5 – 1.5	9416.7601(5)	0.2	9534.9415(5)	0.3
	2.5 – 1.5	9420.3982(5)	–0.1	9536.4093(5)	–0.4
	0.5 – 1.5	9423.2923(5)	–0.1	9537.5667(5)	0.1
$2_{0,2} - 1_{0,1}$	1.5 – 0.5	18829.8453(10)	–0.9	19064.3399(10)	–0.8
	2.5 – 2.5	18830.2219(10)	0.1	19064.5136(10)	–0.4
	0.5 – 0.5	18833.3759(10)	–0.5	19065.7233(15)	–0.1
	3.5 – 2.5	18833.7667(5)	0.0	19065.9120(5)	0.2
	2.5 – 1.5	18833.8607(10)	0.5	19065.9827(5)	0.2
	1.5 – 1.5	18836.3793(10)	0.6	19066.9656(10)	–0.5
$6_{1,6} - 5_{0,5}$	4.5 – 3.5	88112.555(40)	14.	—	
	7.5 – 6.5	88114.215(30)	8.	—	
	5.5 – 4.5	88118.942(40)	–47.	—	
	6.5 – 5.5	88120.679(50)	28.	—	



Table 9  
Molecular Parameters of  $^{33}\text{SSO}$  and  $\text{S}^{33}\text{SO}$  (in MHz).

Parameter	$^{33}\text{SSO}$		$\text{S}^{33}\text{SO}$	
	Prediction <sup>a</sup>	Experiment	Prediction <sup>a</sup>	Experiment
$A$	41823.2	41823.33(35)	41254.7	41255.7108 <sup>b</sup>
$B$	4978.0	4978.0325(175)	5046.6	5046.6177(154)
$C$	4441.7	4441.6424(172)	4489.5	4489.5028(151)
$\Delta_J \times 10^3$		1.8365 <sup>b</sup>		1.8733 <sup>b</sup>
$\Delta_{JK} \times 10^3$		-31.461 <sup>b</sup>		-30.764 <sup>b</sup>
$\Delta_K$		1.1914 <sup>b</sup>		1.1612 <sup>b</sup>
$\delta_J \times 10^3$		0.33073 <sup>b</sup>		0.34495 <sup>b</sup>
$\delta_K \times 10^3$		12.17 <sup>b</sup>		12.19 <sup>b</sup>
$\chi_{aa}$	-15.6	-14.5260(14)	-5.4	-5.8442(14)
$\chi_{bb}$	33.7	33.90(13)	22.0	22.21(15)
$\chi_{cc}$	-18.1	-19.37(13) <sup>c</sup>	-16.6	-16.37(15) <sup>c</sup>
$(C_{bb} + C_{cc})/2 \times 10^3$		2.84(14)		2.98(14)

<sup>a</sup> Rotational constants from  $r_{I,\epsilon}$  structure, nuclear quadrupole coupling constants from B3LYP/cc-pCVTZ calculation (see Sec. 3.3).

<sup>b</sup> Constrained (see Sec. 3.3).

<sup>c</sup> Derived via  $\chi_{aa} + \chi_{bb} = -\chi_{cc}$ .

Table 10

Experimental microwave transition frequencies of  $\text{S}_2\text{O}_2$  (MHz) and residuals  $o - c$  (in kHz).

Transition	Frequency	$o - c$
$2_{1,1} - 2_{0,2}$	11013.8404(20)	0.4
$4_{1,3} - 4_{0,4}$	14081.6402(20)	0.1
$1_{1,1} - 0_{0,0}$	15717.9463(20)	0.6
$4_{0,4} - 3_{1,3}$	16714.1670(20)	-1.1
$3_{1,3} - 2_{0,2}$	26342.8174(20)	0.0
$4_{2,2} - 4_{1,3}$	26553.9151(30)	-3.5
$2_{2,0} - 2_{1,1}$	28493.0459(20)	-0.8
$6_{0,6} - 5_{1,5}$	30629.2832(30)	-0.6
$5_{2,4} - 5_{1,5}$	35295.1993(30)	0.2
$5_{1,5} - 4_{0,4}$	35794.5274(20)	1.4

Table 11  
 Rotational Constants of S<sub>2</sub>O<sub>2</sub> (in MHz).

Parameter	Ref. [21] <sup>a</sup>	Present study + Ref. [21]
$A$	12972.9557 (93)	12972.93037(72)
$B$	3488.9771 (28)	3488.96986(33)
$C$	2745.0589 (30)	2745.05543(20)
$\Delta_J \times 10^3$	3.3823(99)	3.3717(44)
$\Delta_{JK} \times 10^3$	-26.770(89)	-26.926(35)
$\Delta_K \times 10^3$	96.863(77)	96.921(38)
$\delta_J \times 10^3$	1.0367(43)	1.0313(17)
$\delta_K \times 10^3$	6.11(12)	6.158(83)
$\Phi_J \times 10^9$	15.7(50)	13.9(24)
$\Phi_{JK} \times 10^6$	0.153(62)	0.087 (30)
$\Phi_{KJ} \times 10^6$	-0.82 (19)	-0.89(15)
$\Phi_K \times 10^6$	3.41 (45)	3.51(43)
$\phi_J \times 10^9$	-8.4(26)	-11.5 (11)
wrms <sup>b</sup>	0.72	0.82

<sup>a</sup> Refitted.

<sup>b</sup> Weighted rms (dimensionless).

Table 12

Frequency predictions for energetically higher vibrational satellites of S<sub>2</sub>O not investigated in the present study (in MHz).

Transition	(0, 9, 0)	(0, 10, 0)	(0, 5, 1)	(0, 6, 1)
1 <sub>0,1</sub> – 0 <sub>0,0</sub>	9508.900(2)	9501.612(3)	9493.257(1)	9486.727(2)
2 <sub>1,2</sub> – 1 <sub>1,1</sub>	18404.642(18)	18383.544(28)	18402.361(4)	18382.430(8)
2 <sub>0,2</sub> – 1 <sub>0,1</sub>	19011.178(3)	18996.574(6)	18980.095(2)	18966.991(4)
2 <sub>1,1</sub> – 1 <sub>1,0</sub>	19631.216(22)	19623.175(34)	19570.880(6)	19564.703(11)
Transition	(0, 0, 2)	(0, 1, 2)	(0, 2, 2)	(1, 1, 0)
1 <sub>0,1</sub> – 0 <sub>0,0</sub>	9479.852(1)	9474.336(1)	9468.623(1)	9539.030(0)
2 <sub>1,2</sub> – 1 <sub>1,1</sub>	18413.250(2)	18395.049(2)	18376.488(2)	18517.789(1)
2 <sub>0,2</sub> – 1 <sub>0,1</sub>	18953.632(1)	18942.535(1)	18931.046(1)	19071.706(1)
2 <sub>1,1</sub> – 1 <sub>1,0</sub>	19506.323(1)	19502.472(2)	19498.190(2)	19638.508(1)
Transition	(1, 2, 0)	(1, 0, 1)	(1, 1, 1)	(2, 0, 0)
1 <sub>0,1</sub> – 0 <sub>0,0</sub>	9533.204(1)	9501.473(1)	9495.893(1)	9523.095(1)
2 <sub>1,2</sub> – 1 <sub>1,1</sub>	18499.185(1)	18452.327(1)	18434.091(1)	18491.405(2)
2 <sub>0,2</sub> – 1 <sub>0,1</sub>	19059.997(1)	18996.718(1)	18985.495(1)	18985.495(1)
2 <sub>1,1</sub> – 1 <sub>1,0</sub>	19633.818(1)	19553.730(1)	19549.656(1)	19601.137(2)

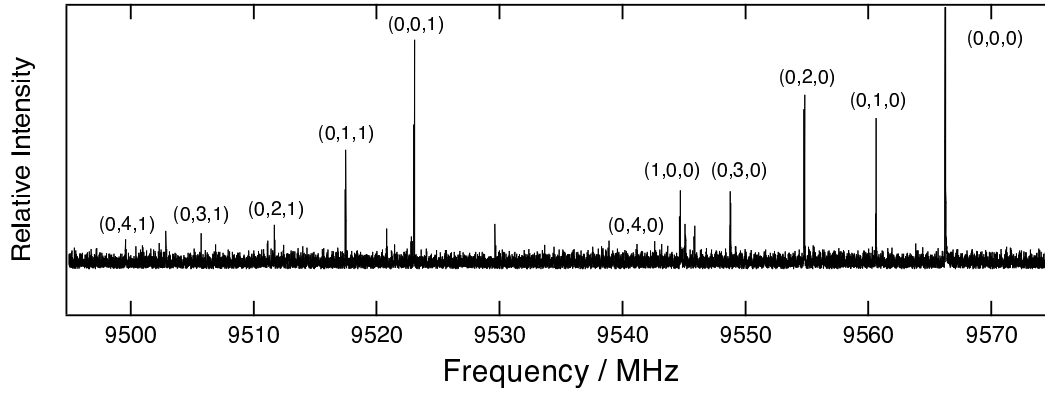


Fig. 1. Vibrational satellite pattern of the  $1_{0,1} - 0_{0,0}$  transitions of  $S_2O$ . The vibrational states are designated according to  $(v_1, v_2, v_3)$ . The spectrum is a composite of single spectra recorded with a step size of 400 kHz. 250 cycles were averaged at each setting of the Fabry-Perot cavity employing a repetition rate of 6 Hz.

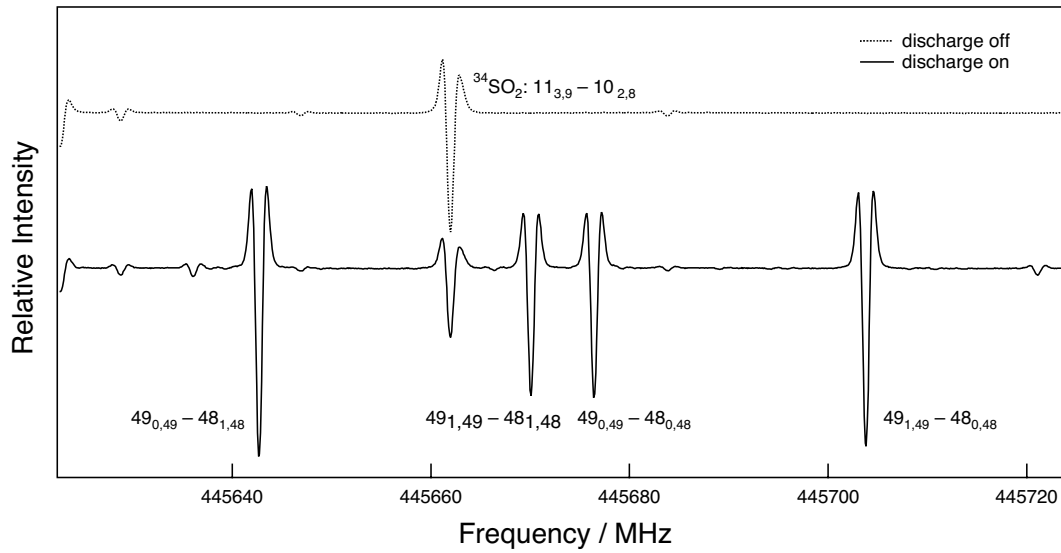


Fig. 2. Submillimeter-wave rotational spectrum of  $\text{S}_2\text{O}$  at 446 GHz. The upper (dotted) spectrum was obtained under experimental conditions with the discharge turned off while the lower spectrum demonstrates the presence of  $\text{S}_2\text{O}$  by four  $J = 49 - 48$  transitions with the discharge on.

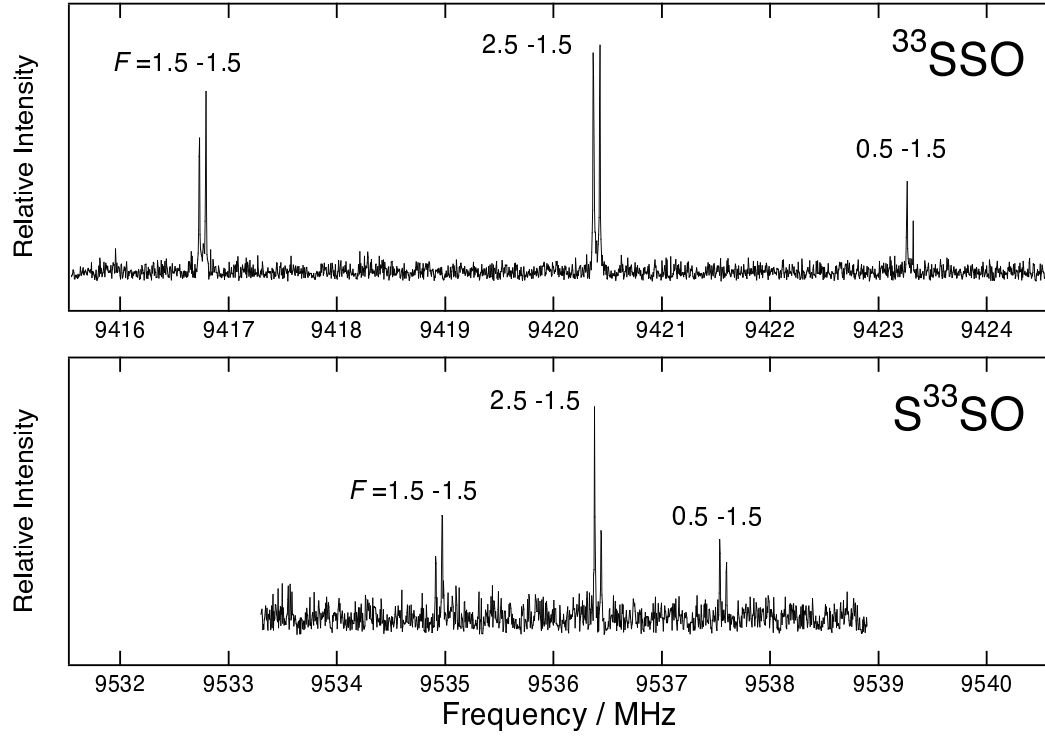


Fig. 3. The  $1_{0,1} - 0_{0,0}$  transitions of  $^{33}\text{SSO}$  (upper) and  $\text{S}^{33}\text{SO}$  (lower) exhibiting hyperfine structure from the  $^{33}\text{S}$  nucleus. The spectra are composites of single spectra recorded with a step size of 400 kHz. 1500 cycles were averaged at each setting of the Fabry-Perot cavity employing a repetition rate of 6 Hz.